JOINT INSTITUTE FOR NUCLEAR RESEARCH
Bogoliubov Laboratory of Theoretical Physics

FINAL REPORT ON THE SUMMER STUDENT PROGRAM

Computer simulation of tunneling characteristics of superconducting nanostructure

Supervisor:
Dr. Prof. Yury M. Shukrinov
Student:
Majed Abdel Salam Nashaat
Cairo University

Participation period:
July 15 – September 10

Dubna, 2017

Contents

Abstract

In this study, superconductor ferromagnetic junction under circularly polarized RF-magnetic field in xy-plane is considered. The order parameter in ferromagnetic is the magnetization and the collective modes are spin waves, which can be excited using the RF-magnetic field. Since the energy levels in ferromagnet are Zemman splitting, the absorption of energy from the oscillating magnetic field at frequency (Ω) corresponding to transitions between the splinting energy states with frequency (Ω_o) leads to ferromagnetic resonance (FMR). On other hand, in superconductor the order parameter is the condensate, which has a phase. Voltage will be generated from the dynamics of this phase. Due to magnetic field, the phase should be a gauge invariant. As a result, a modified RCSJ equation is found. In this new frame the interaction of spin wave magnons and singlet cooper pairs of the superconductors are considered. The dynamics of the magnetization components and the trajectory of the total magnetization in space (Bloch sphere) are described by Landau-Lifshitz-Gilbert (LLG) equation. We solve numerically a system of equations which couples the RCSJ with the LLG equations. The IV-characteristics shows new features at FMR. Additional fractional voltage steps appears between the voltage steps due to FMR, when the coupling between the LLG and RCSJ equation is taken into account which is represented by Josephson energy. The dynamics for the magnetizations are studied at different regions in the IV-characteristics with the phase dynamics of the Josephson junction (JJ).

1 Introduction

A fascinating quantum tunneling effect was postulated by *BrainJosephson* in 1962 in which a supercurrent tunnels through an extremely thin layer ($\sim 10\mathring{A}$) of an insulator between two superconductor electrodes. This current is decried by $I = I_c \sin\theta$, I_c is the critical current and θ is the phase difference between the macroscopic wave functions describing the superconducting electrodes [1,2]. Additionally, it found that a supercurrent between two superconductors can tunnel through a normal metal [3] or a ferromagnetic metal [4] by coherent electron hole pairs. In the latter case, the quantum phases of the electrons and the holes are modified by the intrinsic magnetic field of the ferromagnetic layer. The current-phase relation of superconductor/ferromagnetic metal/superconductor (SFS) Josephson junction is shifted by π and reads as $I = I_c \sin(\theta + \pi)$ [5]. These junctions are called π-junctions and define a new building element for spintronics [6].

The central theme of spintronics is the active manipulation of spin degrees of freedom in solid-state systems [7]. One goal of spintronic is to understand the interaction between the particle spin and its solid-state environments, and make useful devices using this acquired knowledge [7]. Fundamental studies of spintronics include investigations of spin transport in electronic materials, spin dynamics and spin relaxation. The possibility of achieving electric control over the magnetic properties of the magnet by the Josephson current and its counterpart, i.e. achieving magnetic control over Josephson current, has recently attracted a lot of attention [5, 8–10]. Spin-orbit coupling plays a major role in achieving such control [11]. For example, in SFS junction, its presence in a ferromagnet without inversion symmetry provides a mechanism for a direct coupling between the magnetic moment and the superconducting current [11]. In such junctions, the time reversal symmetry is broken, and the current-phase relation is given by $I = I_c \sin(\theta - \phi_o)$, where ϕ_o is proportional to the magnetic moment perpendicular to the gradient of the asymmetric spin-orbit potential and also to the applied current [11]. Many questions arise concerning this type of junctions, e.g., if one can generate magnetization reversal and how long the system able to remember its spin orientation?. A recent study shows a full magnetization reversal in SFS with spin-orbit coupling by adding electric current pulse to the system [10]. While others show the interaction of nanomagnet with weak superconducting link and a reversal of single domain magnetic particle by ac field [12, 13].

Another mechanism is considered to describe the coupling between the Josephson current and the magnetization dynamics in different structures (SFS, SIFS or SFIFS,..) [9,14–17]. In the SIS junction [9,18,19], the Josephson plasma waves can propagate in the junctions and their dispersion relation is $\omega^2 = \Omega_J^2 + k^2 v_J^2$, where Ω_J is the Josephson plasma frequency and v_J is the velocity of Swihart waves. While in the F-layer, the dispersion relation is $\omega^2 = \Omega_o^2(1 + k^2 l_m^2)$, where Ω_o is the magnetic resonance frequency and l_m is a magnetic length [20]. Usually $l_m < l_j, (l_j = v_j/\Omega_J)$ and if $\Omega_J < \Omega_o$, both dispersion relations can cross each other [9]. The interaction between magnetization and Josephson currents leads to a coupling between Josephson plasma and spin waves. Since the energy levels in ferromagnet are Zemman splitting, the absorption of energy from the oscillating magnetic field at frequency (Ω) corresponding to transitions between

the splitting energy states with frequency (Ω_o) leads to ferromagnetic resonance (FMR). In this case the uniform magnetization of a ferromagnetic sample is excited by a uniform external microwave field with frequencies in the GHz regime. In [16], the authors consider SFS junction with zero McCumber parameter at FMR. The IV-characteristic demonstrates voltage step at even power of the frequency of the RF-magnetic field. The reason for these steps are due to the interaction between cooper pairs and magnons [16].

Magnetization dynamics are characterized by nonlinear behavior. However, one need to drive a system above some threshold power to see these nonlinear dynamics. In this case, there is sufficient energy going in as to counteract the natural losses or damping from the magnetic system. If driven far enough into the nonlinear regime, magnetic systems may display chaotic behavior. That is, very small changes in the initial magnetization conditions lead to vastly different dynamics [21]. Spin torque nano-oscillators and other novel spintronic devices their operation can be affected by nonlinear effects. Nonlinear damping of the magnetization vector motion becomes more important to consider in order to understand the resulting dynamics and to optimize a device performance. In some cases, the nonlinear effects are in fact desirable and allow for the design of signal processing devices such as frequency modulators or filters that operate in the microwave regime [21].

In the current study, we consider the effect of magnons on Josephson phase, and its counterpart in the frame of the RCSJ model with over-damped case ($\beta_c = 0$). Due to this coupling, new features appear in the IV-characteristic for SFS junction. An additional fractional voltage steps between the ferromagnetic resonance voltage steps appear. The position of these steps follow continued fraction formula similar to that demonstrated in [22] for SIS structure. Thus the coupling between Josephson phase and magnons opens the gate for the synchronization between the applied magnetic field frequency and the Josephson frequency. Fast Fourier transform shows that large angle of precession for the magnetization component occur. Each time the magnetization passes through a region, its trajectory is changing, opening up new loops on the Bloch sphere. The motion does not trace out the same loop each period. Such chaotic motion can be induced by the Josephson current which affect the magnetization precession which is determined by LLG equation.

1.1 Theory of Josephson Tunneling

The Josephson effect is a quantum tunneling effect which was first predicted from theory and later it was observed in experiments [23]. According to quantum mechanics, if two metals are brought very close, but still with a small gap in between, there is a chance that an electron of the one metal is found in the other metal "electron tunnelling". By applying a potential difference, a current can flow from the one metal to the other, even though there is an insulator in between. Similarly the Josephson effect occurs, if two superconductors are brought close to each other.

In ideal superconductors, all electrons condense to the superconducting state, i.e., they form Cooper pairs and they are in the same state. When two superconductors are brought together with a weak link in between, a finite overlap of the macroscopic wave-function of the two weakly coupled superconductors can occur which means that a Cooper pair tunneling takes place (see fig 1).

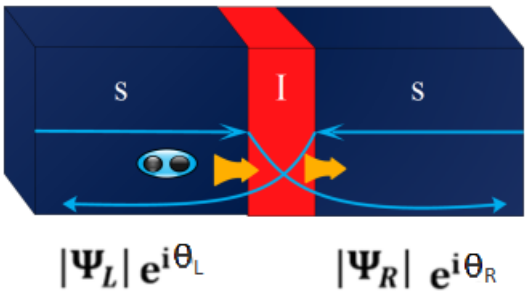

Figure 1: Two superconductors separated by a thin insulating barrier

Derivation of the 1^{st} and the 2^{nd} Josephson equations:

In order to understand the electrical performance of Josephson junctions, it is beneficial to comprehend the Josephson equations. By applying a voltage V across the junction, the potential of the left side is raised with respect to the right side. The energy for the electrons is lower at the left, since the electron has a negative charge. For simplicity, the zero of energy can be taken midway between the two energies, so that $E_L = -E_R = -eV$. The Schrödinger equations for this system are then given by:

$$i\hbar\frac{\partial\Psi_L}{\partial t} = -eV\Psi_L - K\Psi_R \tag{1a}$$

$$i\hbar\frac{\partial\Psi_R}{\partial t} = eV\Psi_R - K\Psi_L, \tag{1b}$$

where Ψ_i (i=R or L) represents the single wave function for the cooper pairs, and K represents the coupling interaction coefficient between the two superconductors and depends on the structure of the junction. We can express the complex wave function for each superconductor in terms of a magnitude and a phase (θ):

$$\Psi_L = \sqrt{n_L}e^{i\theta_L} \qquad and \qquad \Psi_R = \sqrt{n_R}e^{i\theta_R}, \tag{2}$$

where n_i (i=R or L) is the density of the pairs. Substituting Eq.(2) into Eq.(1), and introduce $\theta = \theta_L - \theta_R$ after separating the real and the imaginary parts, the time evolution equations are:

$$\frac{\partial n_L}{\partial t} = \frac{2}{\hbar}K\sqrt{n_L n_R}\sin\theta \tag{3a}$$

$$\frac{\partial n_R}{\partial t} = -\frac{2}{\hbar}K\sqrt{n_L n_R}\sin\theta \tag{3b}$$

$$\frac{\partial\theta_L}{\partial t} = \frac{K}{\hbar}\sqrt{\frac{n_R}{n_L}}\cos\theta + \frac{eV}{\hbar} \tag{4a}$$

$$\frac{\partial\theta_R}{\partial t} = \frac{K}{\hbar}\sqrt{\frac{n_L}{n_R}}\cos\theta - \frac{eV}{\hbar} \tag{4b}$$

From Eq.(3), we notice that the magnitude of the rate of decreasing the pair density in one superconductor is the same as the rate of increasing the pair density in the other superconductor. The time derivative of the density of Cooper pairs describes a charge transport; this means that $J = \dot{n}$, where $\dot{n}$ is the time derivative of the density. The energy levels will shift according to $E_L - E_R = 2eV$, where $2e$ is the charge of a cooper pair. At this stage we can deduce two Josephson effects:

- **The DC Josephson effect**
  Eq.(3) can be written as:

$$I_s(\varphi) = I_c \sin(\theta), \tag{5}$$

  where I_s is the supercurrent density, and $I_c = 2K/\hbar\sqrt{n_L n_R}$ is the critical current density. The maximum Josephson current density that can flow through the barrier determined by the Cooper pair density. This equation takes a value between $-I_c$ and $+I_c$. It correlates the phase difference at the Josephson contact with the current of the Cooper pairs across this contact. The maximum energy exchange will take place for a phase shift of $\pm\pi/2$. A dc current applied to Josephson junction by external source, results in a constant phase difference for $-I_c \leq I \leq I_c$:

$$\theta = \theta_n = \arcsin\left(\frac{I}{I_c}\right) + 2\pi n, \qquad \theta = \widetilde{\theta}_n = \pi - \arcsin\left(\frac{I}{I_c}\right) + 2\pi n \tag{6}$$

  The constant phase means that $d\theta/dt = 0$. Each of the solutions corresponds to zero junction voltage and describes the superconducting state. This case is called the zero voltage state [18].

- **The AC Josephson effect**
  Subtracting Eq.(4.a) from Eq.(4.b), we get

$$\frac{d\theta}{dt} = \frac{2e}{\hbar}V \tag{7}$$

  Consequently, the phase difference changes linearly with time in case of a potential difference between both superconductors [18]. Accordingly, the $L.H.S$ has the unit of frequency, and $2e/h = 483.6MHz/\mu V$, this frequency lies in most cases in the microwave regime for experimentally achievable voltages. According to this, the Ac Josephson effect can be illustrated as follows; due to the presence of the voltage, the tunneling Cooper pairs are accelerated and gain energy $2eV$, as they are not allowed to alter their energy while tunneling a photon of the energy $hf = 2eV$ is emitted .

1.2 Gauge Invariance for the Josephson Effect

The phase difference should be redefined so that the current density is gauge invariant under the choice of the mathematical formulation for any magnetic field which may be existed. For two points (a_1, a_2) shown in Fig.2, the gauge change for a vector potential $\mathbf{A}$ is:

$$\mathbf{A}' = \mathbf{A} + \nabla\chi, \tag{8}$$

where χ is an arbitrary scaler function. The phase at the two points:

$$\theta'_{1,2} = \theta_{1,2} - \frac{2e}{\hbar}\chi_{1,2} \tag{9}$$

While the phase difference defined as:

$$\theta = \theta_1 - \theta_2 + \frac{2e}{\hbar}\int_1^2 \mathbf{A}(x,t)\cdot dl \tag{10}$$

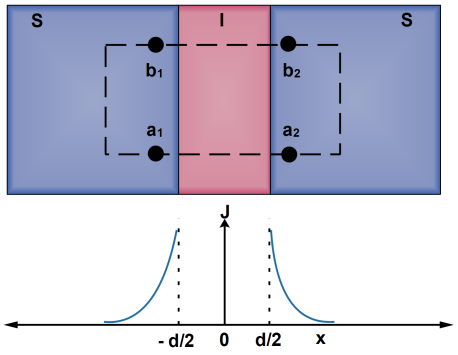

Figure 2: The integration contour for the vector potential $\mathbf{A}$

According to this, θ is independent of the choice of χ i.e., the choice of the gauge under the substitution of Eqs.(8, 9). The relation between the phase difference and the magnetic field passing through a junction in the plane of the barrier can be found as follows: Consider four points along the junction (see Fig.2). The gauge is the London gauge, where the phase gradient is zero inside each of the two superconductors (electrodes.). Then θ_1 is the same at a_1 and b_1, and θ_2 is the same at a_2 and b_2. Using Eq.(10):

$$\theta_b - \theta_a = \frac{2e}{\hbar}\left(\int_{b_1}^{b_2}\mathbf{A}'(b,t)\cdot dl - \int_{a_1}^{a_2}\mathbf{A}'(a,t)\cdot dl\right) \tag{11}$$

The magnetic flux (outward-direction) through the rectangular contour is:

$$\Phi_y = \int_s \mathbf{B}\cdot ds = \oint \mathbf{A}'\cdot d\mathbf{l} = \int_{a_1}^{a_2}\mathbf{A}'\cdot d\mathbf{l} + \int_{a_2}^{b_2}\mathbf{A}'\cdot d\mathbf{l} + \int_{b_2}^{b_1}\mathbf{A}'\cdot d\mathbf{l} + \int_{b_1}^{a_1}\mathbf{A}'\cdot d\mathbf{l}, \tag{12}$$

where $\mathbf{B}$ is the magnetic field. As the canonical momentum in the transformed gauge is $\mathbf{p}' = e^*\Lambda\mathbf{J}_s + e^*\mathbf{A}'$, $\mathbf{p}' = \hbar\nabla\theta'$, and Λ is the London coefficient. As $\nabla\theta' = 0$ in the superconductors, then $\Lambda\mathbf{J}_s = -\mathbf{A}'$ [24]. This means that; the integrals in Eq.(12) are equivalent to integrals of the current density. Since the current is parallel to the junction surface, those portions of the contour that are perpendicular to the surface make no significant contribution to the integrals. In addition to this, if the superconductors thickness is much larger than the

penetration depth, the second and the last integral can be neglected. The final expression is:

$$\theta_b - \theta_a = \frac{2e}{\hbar}\Phi_y \tag{13}$$

This means that; the difference of the phase differences between these two points along a junction is proportional to the magnetic flux passing through the junction between the points. If we suppose that the points a and b are separated by a differential distance dz, the flux will be function of; the flux in the barrier (insulator) B_y^b, the penetration depth of the two superconductors λ_1, λ_2, and the barrier thickness d.

$$\Phi_y = B_y^b(\lambda_1 + \lambda_2 + d)dz \tag{14a}$$

$$\frac{\partial\theta}{\partial z} = \frac{2e}{\hbar}B_y^b(\lambda_1 + \lambda_2 + d) \tag{14b}$$

$$\frac{\partial\theta}{\partial y} = -\frac{2e}{\hbar}B_z^b(\lambda_1 + \lambda_2 + d) \text{ If they are separated in the y-direction.} \tag{14c}$$

Generally:

$$\nabla\theta = \frac{2ed'}{\hbar}\left[\mathbf{B}^b(\mathbf{r}, t) \times \mathbf{n})\right], \tag{15}$$

where $\mathbf{n}$ is the unit vector directed from one superconductor toward the other.

1.3 Resistively and Capacitively Shunted Junction (RCSJ)

The basic idea in the RCSJ model is to describe the Josephson junction with an equivalent circuit for Josephson junction. The circuit contains a capacitor, a resistor, and the Josephson supercurrent in a parallel configuration (see Fig3a). The model was introduced by *W.C.Stewart* and *D.E.McCumber* to describe the current voltage characteristics for Josephson junction [25, 26].

According to this model we have:

- I_s: accounts for the supercurrent with current density J_s.

  $$I_s = I_c \sin\theta \tag{16}$$

  According to $V = LdI/dt$, and L is the inductance, we can get the inductance for Josephson junction as follows:

  $$V = L_s\frac{dI_s}{dt} \tag{17}$$

  Using $I_s = I_c \sin\theta(t)$, then

  $$L_s = \frac{L_c}{\cos\theta(t)}, \tag{18}$$

  where

  $$L_c = \frac{\hbar}{2eI_c} \tag{19}$$

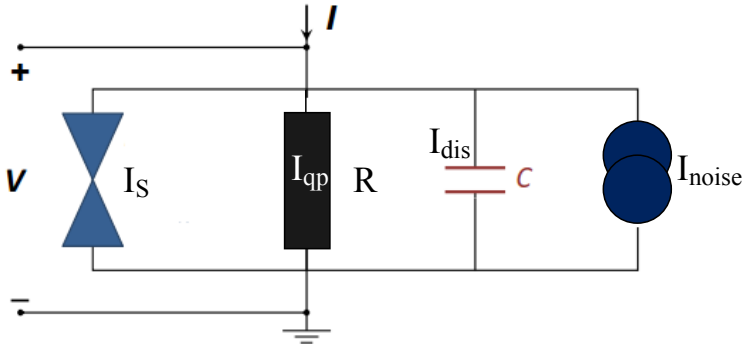

(a)

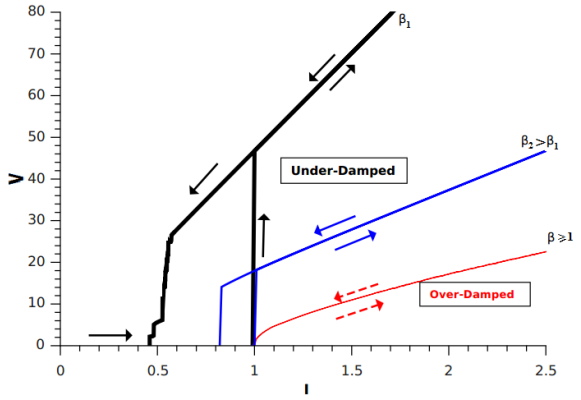

(b)

Figure 3: **a)**Equivalent circuit for Josephson junction, **b)** Current voltage characteristic for Josephson junction.

- **Conductance**: represents the quasi-particle current. At finite temperatures ($T > 0$) there is a finite density of normal electrons due to thermal break-up of Cooper pairs. The presence of the condensate of paired electrons makes the properties of these normal excitations somewhat different from those in the normal state they are usually called quasi-particles. In the superconducting state, where the voltage across the Josephson junction equals zero, the quasi-particles do not contribute to its current. If, however, the Josephson phase φ changes in time and the voltage is non-vanishing, then a quasi-particle current appears. If T is close to the critical temperature T_c of a superconductor, the binding energy 2Δ,(Δ is the gap energy of the superconductor) of the Cooper pair becomes much smaller than the thermal energy K_BT, where k_B is the Boltzmann constant. As a result, the concentration of Cooper pairs is small, and the concentration of normal electrons is close to its value in the normal state (at $T > T_c$). In this case, the I_{qp}-V dependence is close to the usual Ohm's law:

$$I_{qp} = G_N V, \tag{20}$$

where $G_N = R^{-1}$ is the normal conductance of the Josephson junction.

While if the voltage across the junction is above the gap value, a Cooper pair in one of the electrodes breaks and one of the two newly formed quasi-particles passes to another electrode. The I_{qp}-V dependence is close to the Ohmic dependence at all temperatures [18].

- **Capacitor**: carries the displacement current, which flows between the adjacent superconducting electrodes.
  - The capacitance depends on the junction type and its size. For a planar tunnel junction it is given by $\epsilon\epsilon_o A/d$, where A is the junction area, d is the insulating thickness, and ϵ is the dielectric constant of the barrier (insulator) material.

  For most practical junctions the displacement current can be represented in the usual form:
  $$I_{dis} = C\frac{dV}{dt}, \tag{21}$$
  where C is the junction capacitance, which is the same in the normal and the superconducting state. In practice the relative magnitude of the displacement current I_{dis} is of importance rather than the absolute value of C.

  An estimation for the above currents with respect to the voltage show that $I_s \precsim V/\omega L_c$, $I_{qp} \precsim VG_N$, and $I_{dis} \approx \omega CV$ [18].

- **Noise current source**: represents the fluctuation in the current.

Due to the conservation of charge, an input current must be in balance with the current through the junction. The total current is the sum of the Josephson-current I_s, the quasi-particle current I_{qp} and the displacement current I_{dis}.

RCSJ current:
$$I = I_c \sin\theta + \frac{V}{R} + C\frac{dV}{dt} + I_{noise} \tag{22}$$

Using equ.7:
$$I = I_c \sin\theta + \frac{\hbar}{2eR}\dot{\theta}(t) + \frac{\hbar C}{2e}\ddot{\theta}(t) + I_{noise} \tag{23}$$

The following characteristic frequencies (times) and parameters are defined in order to study the dynamics of the phase and the voltage for Josephson junction:

- **Plasma frequency**: The charge is oscillating back and forth as in a plasma mode. The Josephson plasma oscillation is analogous to the bulk plasma oscillation in the same way. From the wave equation for a Josephson tunnel junction it was found that [27]:
$$\omega_p = \tau_p^{-1} = \sqrt{\frac{2eI_c}{\hbar C}} \tag{24}$$

- **Time constant of the equivalent circuit**: Is the inverse relaxation time in a system consisting of a normal current and a supercurrent.

$$\omega_c = \tau_c^{-1} = \frac{R}{L_c} = \frac{2eI_cR}{\hbar}, \tag{25}$$

where I_cR is known as the characteristic voltage of Josephson junction. At $V < V_c$ the normal current is smaller than the critical junction current.

- **RC time constant of the equivalent circuit**:

$$\omega_{RC} = \tau_{RC}^{-1} = \frac{\omega_p^2}{\omega_c} = \frac{1}{RC} \tag{26}$$

- **Stewart-McCumber parameter** β_c: corresponds to the square of the quality factor Q of a parallel LRC circuit. It compares the decay time constant of the amplitude of an oscillating physical system to its oscillation period.

$$\beta_C = \frac{\omega_p^2}{\omega_c^2} = \frac{2eJ_cCR^2}{\hbar} = \frac{\tau_{RC}}{\tau_J}, \qquad Q = \frac{RC}{\sqrt{LC}} = \frac{\omega_c}{\omega_p} = \frac{\omega_p}{\omega_{RC}}, \tag{27}$$

where τ_{RC} is the capacitor time constant, and $\tau_J = \hbar/2eJ_cR$ is the characteristic time associated with the phase evolution across the JJ. Starting from zero applied current and then increasing the current, the JJs stay in the zero voltage state in both cases until the critical current is reached. After that, the JJs go to the resistive state. Now when the current start to decrease, we can differentiate between the two cases; in the over-damped case; $\beta_c << 1$, the time required for the charge on the capacitor to relax is much shorter than τ_J, this means that; we can neglect the effect of the capacitor and the current voltage characteristics (CVC) has no hysteresis. While in the under-damped case; $\beta_c >> 1$, τ_J is much shorter than τ_{RC}, and when the biasing current start to decrease, a voltage can still be maintained since it takes a long time for the voltage across the capacitor to relax, the Josephson oscillations occur and the CVC has a hysteresis, where its size is affected by the values of β_c in the under-damped case, as shown in Fig3b.

1.4 Landau-Lifshitz-Gilbert Equation

In an atom the electron has two angular momenta: the orbital ($\mathbf{L}$) and spin ($\mathbf{S}$) angular momentum. The corresponding magnetic moments are $\boldsymbol{\mu}_l$ and $\boldsymbol{\mu}_s$ respectively:

$$\begin{aligned} \boldsymbol{\mu}_L &= -\gamma_L \mathbf{L} \\ \boldsymbol{\mu}_S &= -\gamma_S \mathbf{S} \end{aligned} \tag{28}$$

where γ_L and γ_S represent the orbital and the spin gyromagnetic factors. Which can be expressed in terms of Planck's constant ($\hbar$), Bohr magnetron ($\mu_B =$

$|e|\hbar/2m_e$ where e and m_e is the charge and the mass of the electron) and the gyromagnetic splitting factor, g_L or g_S:

$$\gamma_{L,S} = g_{L,S}\frac{\mu_B}{\hbar} \tag{29}$$

If one consider an arbitrary external magnetic field (**H**), the rate of change of the electron magnetic moment μ to the torque exerted on the particle by the magnetic field is given by:

$$\frac{d\boldsymbol{\mu}}{dt} = -\gamma\boldsymbol{\mu} \times \mathbf{H} \tag{30}$$

The frequency of precession is the Larmor frequency $f = \gamma H/2\pi$.

Spins in ferromagnetic materials are strongly coupled by the exchange interaction [28]. So, there is no strong variation of the orientation of the magnetic moments from one lattice site to the next. Then one can introduce the average of magnetic moment, called magnetization,**M**, by taking the volume average of both sides of the equation.30, one has:

$$\frac{d\mathbf{M}}{dt} = -\gamma\mathbf{M} \times \mathbf{H} \tag{31}$$

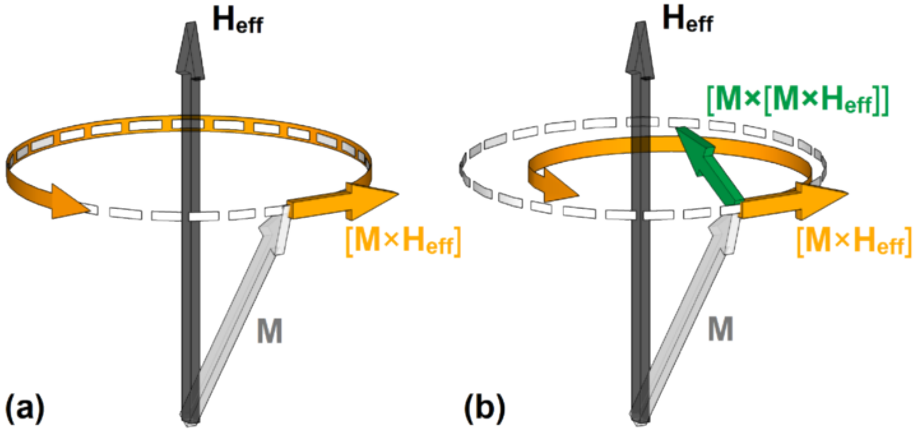

Figure 4: Magnetization precession for (a) undamped motion and (b) motion with damping.

The first dynamical model for the precessional motion of the magnetization was proposed by Landau and Lifshitz in 1935:

$$\frac{d\mathbf{M}}{dt} = -\gamma\mathbf{M} \times \mathbf{H}_{eff} \tag{32}$$

In the frame of the micromagnetism theory, spontaneous magnetization is excised and its vector has a constant amplitude $|\mathbf{M}| = const$. The effective magnetic field in equation .32 is given by the derivative of the total energy of the ferromagnetic system:

$$\mathbf{H}_{eff} = -\nabla_M E \tag{33}$$

where E is the total energy of a magnetic system and it has different contributions coming from exchange energy, magneto-crystalline anisotropy energy,

dipolar energy, Zeeman energy and other quantum effects [29]. The approach followed by Landau and Lifshitz consists of introducing dissipation in a phenomenological way. They introduce an additional torque term that pushes magnetization in the direction of the effective field (see Fig.**??**). Then, the Landau-Lifshitz equation becomes:

$$\frac{d\mathbf{M}}{dt} = -\gamma \mathbf{M} \times \mathbf{H}_{eff} - \frac{\lambda}{M_s} \mathbf{M} \times \mathbf{M} \times \mathbf{H}_{eff} \tag{34}$$

where $\lambda > 0$ is a phenomenological constant characteristic of the material and M_s is the saturation magnetization.

In 1955 Gilbert proposed different approach for phenomenological dissipation by introducing a kind of 'viscous' force, whose components are proportional to the time derivatives of the generalized coordinates of the magnetization. [30]. He introduces the following torque term:

$$\frac{\alpha}{M_s} \mathbf{M} \times \frac{d\mathbf{M}}{dt} \tag{35}$$

where $\alpha > 0$ is the Gilbert damping constant, depending on the material. Therefore, the precessional equation, modified according to Gilbert's work, is generally referred to as Landau-Lifshitz-Gilbert equation:

$$\frac{d\mathbf{M}}{dt} = -\gamma \mathbf{M} \times \mathbf{H}_{eff} + \frac{\alpha}{M_s} \mathbf{M} \times \frac{d\mathbf{M}}{dt} \tag{36}$$

Using the vector identity $\mathbf{a} \times (\mathbf{b} \times \mathbf{c}) = \mathbf{b}(\mathbf{a} \cdot \mathbf{c}) - \mathbf{c}(\mathbf{a} \cdot \mathbf{b})$ and $\mathbf{M} \cdot \frac{\partial \mathbf{M}}{\partial t} = 0$ ($|M| = const$) one ends with:

$$\frac{d\mathbf{M}}{dt} = -\frac{\gamma}{1+\alpha^2} \mathbf{M} \times \mathbf{H}_{eff} - \frac{\gamma\alpha}{(1+\alpha^2)M_s} \mathbf{M} \times (\mathbf{M} \times \mathbf{H}_{eff}) \tag{37}$$

equation.34 and 37 are mathematically equivalent if one assumes:

$$\gamma \longmapsto \frac{\gamma}{1+\alpha^2}, \qquad \lambda \longmapsto \frac{\gamma\alpha}{1+\alpha^2} \tag{38}$$

2 Model

Consider two superconductors separated by ferromagnetic layer with thickness d. The area of the junction is $l_y l_z$ see Fig.5. A bias current is applied in x-direction, and microwave radiation is applied to the junction. The magnetic field is assumed to be circularly polarized in the xy-plane with amplitude h_{ac} and frequency Ω. The components of the magnetic field are $(h_{ac} \cos \Omega t, h_{ac} \sin \Omega t, 0)$. While the electric field $(A \sin \Omega t)$ with amplitude A and frequency Ω is assumed to be in the x-direction. If the superconductors are thicker than the London's penetration depth, the magnetic field generated by Josephson current can be neglected.

In the RCSJ model [25, 26], the phase difference θ(t) between the superconductors is described by:

$$I = I_c \sin \theta(t) + \frac{\Phi_o}{2\pi R} \frac{d\theta(t)}{dt} + C \frac{\Phi_o}{2\pi} \frac{d^2\theta(t)}{dt^2} \tag{39}$$

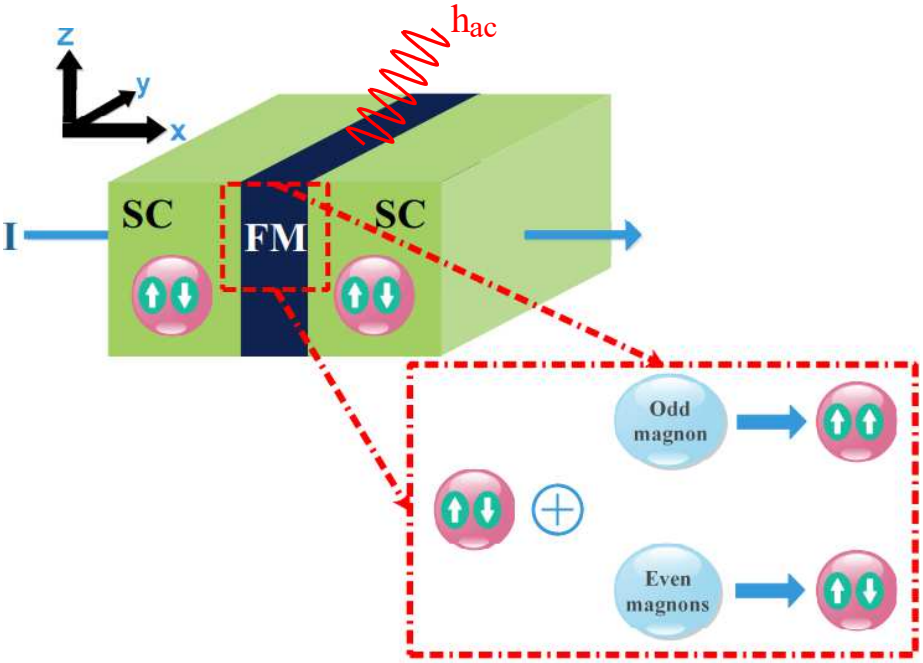

Figure 5: SFS Josephson junction. The bias current is in x-direction. Circularly polarized microwave with amplitude h_{ac} and frequency Ω is applied in x-y plane. The enlarged part show the results of the interaction between cooper pairs from superconductor and magnons (spin wave) inside ferromagnetic layer.

where I_c is the critical current, Φ_o is the flux quantum (h/2e), R and C are the resistance, and the capacitance in the Josephson junction respectively. The applied microwave causes precessional motion of the magnetization in the ferromagnetic (FM) layer. As a result, an excitation of the uniform mode of a spin wave is occurred. The dynamics of magnetization due to the microwave radiation is described by the Landau-Lifshitz-Gilbert (LLG) equation [31]:

$$(1+\alpha^2)\frac{d\mathbf{M}}{dt} = -(\gamma\ \mathbf{M}\times\mathbf{H}_{eff} + \frac{\gamma\ \alpha}{|\mathbf{M}|}\left[\mathbf{M}\times(\mathbf{M}\times\mathbf{H}_{eff})\right]) \tag{40}$$

where H_{eff} is the effective field which contains; 1) the external magnetic field, 2) the magnetic field due to the magnetization (demagnetization field); notice that the anisotropic precession of the magnetization due to the this field will be neglected, and 3) other fields due to quantum effects. Due to magnetic field, the phase in the superconductor should be a gauge invariant. As a result, the RCSJ equation should be modified. The magnetic flux in z and y direction are $\Phi_z(t) = 4\pi d l_y M_z(t)$, $\Phi_y(t) = 4\pi d l_z M_y(t)$ (we put $\mu = 1$ permeability). The gauge-invariant phase difference is given by:

$$\theta(y,z,t) = \theta(t) - \frac{8\pi^2 d M_z(t)}{\Phi_o}y + \frac{8\pi^2 d M_y(t)}{\Phi_o}z \tag{41}$$

By integrating over junction area, the modified RCSJ equation [32] reads as:

$$
\begin{aligned}
I/I_c + A\sin\Omega t &= \sin\theta \frac{\sin\left(\frac{\pi\Phi_z(t)}{\Phi_o}\right)\sin\left(\frac{\pi\Phi_y(t)}{\Phi_o}\right)}{(\pi\Phi_z(t)/\Phi_o)(\pi\Phi_y(t)/\Phi_o)} \\
&+ \frac{d\theta(\tau)}{d\tau} + \beta_c \frac{d^2\theta(\tau)}{d\tau^2}
\end{aligned} \tag{42}
$$

where $\tau = t\tau_J$, $\tau_J = \Phi_o/2\pi RI_c$, and $\beta_c = RC/\tau_J$ is the McCumber parameter. Here we consider over-damped case with $\beta_c = 0$. We will assume the amplitude of the electric field $A = 0$.

In [16] the authors consider the effective field in such junction to be in the form of $H_{eff} = H_{ac} + H_o$ where H_o is an uniaxial magnetic anisotropic field which is assumed to be in z direction, and $H_{ac} = (h_{ac}\cos\Omega t, h_{ac}\sin\Omega t, 0)$ is the microwave driving field. In this study, we take into account the Josephson energy part in the total effective field. The total field can be found by follow the same procedure as in Ref's. [10–13]. The effective field will be H_{eff}= H_o+ $H_{ac} - \frac{1}{V}\frac{\partial}{\partial M}\epsilon_J$ where V is the volume, $\epsilon_J = E_J(1-\cos\theta)$ and $E_J = \Phi_o I_c/2\pi$. By defining the following dimensionless parameters:

$m = \dfrac{\mathbf{M}}{|M|}$, $\tau = \frac{t}{\tau_j}$, $\tau_j = \frac{\Phi_o}{2\pi I_c R}$, $h_{T_{eff}} = \frac{H_{T_{eff}}}{H_o}$, $\epsilon_J = \frac{E_J}{V|M|H_o}$, $h_{ac} \longmapsto \frac{h_{ac}}{H_o}$, $\Omega \longmapsto \Omega\tau_j$, $\Omega_o \longmapsto \Omega_o\tau_j$, ϕ_{sy}=$\dfrac{4\pi^2 l_y d|M|}{\Phi_o}$, ϕ_{sz}=$\dfrac{4\pi^2 l_z d|M|}{\Phi_o}$.

where H_o= Ω_o/γ, Ω_o is the ferromagnetic resonance frequency. The LLG in the dimensionless form reads as:

$$
\frac{dm}{d\tau} = -\frac{\Omega_o}{(1+\alpha^2)}\Big(m \times h_{eff} + \alpha\left[m \times (m \times h_{eff})\right]\Big) \tag{43}
$$

The anisotropic precession of the magnetization due to the demagnetization field [33] will be neglected for simplicity. Using Eq.(41) and taking the integration over the junction area, the total effective field in this case $h_{T_{eff}}$ is given by:

$$
\begin{aligned}
h_{T_{eff}} &= h_{ac}\cos\Omega\tau \;\; \hat{e}_x \\
&+ \left(h_{ac}\; sin\Omega\tau + \frac{\epsilon_J(\cos\theta)\sin(\pi\phi_{sy}m_z)}{m_y(\pi\phi_{sy}m_z)}\left[\cos(\pi\phi_{sz}m_y) - \frac{\sin(\pi\phi_{sz}m_y)}{(\pi\phi_{sz}m_y)}\right]\right) \;\; \hat{e}_y \\
&+ \left(1 + \frac{\epsilon_J(\cos\theta)\sin(\pi\phi_{sz}m_y)}{m_z(\pi\phi_{sz}m_y)}\left[\cos(\pi\phi_{sy}m_z) - \frac{\sin(\pi\phi_{sy}m_z)}{(\pi\phi_{sy}m_z)}\right]\right) \;\; \hat{e}_z
\end{aligned} \tag{44}
$$

Using Eq.(43) and Eq.(44) in the dimensionless form, the equation of motions for the magnetization dynamics in x-, y- and z- direction can be determined.

Here, we demonstrate estimations of the numerical parameters that characterize our model. The flux quantum Φ_o=2.067833 * 10 $^{-15}$ Wb, the permeability μ_o= 4*π*10^{-7} $Wb/Amp.m$. In case of junction with d=10 nm, l_y=l_z=20 nm, critical current density $I_c = 6.4 * 10^8$ Amp/m^2, saturation magnetization M=6*10^5 Amp/m, Ω_o=100 GHz and gyromagnetic ration $\gamma = 6\pi$ MHz/T. Then ϕ_{sz}=ϕ_{sy}=2.8, $\epsilon_J = 0.16$. If for example Ω_o=400 GHz then $\epsilon_J = 0.04$. While for junction with d=7 nm, l_y=l_z=30 nm, critical current density I_c=4 $MAmp/m^2$, saturation magnetization M=5.6*10^5 Amp/m, Ω_o=350 GHz and gyromagnetic ratio $\gamma = 8\pi$ MHz/T. Then ϕ_{sz}=ϕ_{sy}=2.8, $\epsilon_J = 1.87$.

3 Results and Discussion

In this section, we demonstrate our results for the self-consistent current-phase relation in SFS junction taking into account the coupling between Josephson phase and magnons in F-layer. We solve Eq.(42) combined with Eq.(43) using the 4^{th} order Runge-Kutta method. As a result, we find the temporal dependence of the voltage $V(t)$, phase $\theta(t)$, and $m_i(t)$ (i=x,y,z) in the SFS junction at a fixed value of the bias current I. Then the current value is increased or decreased by a small amount of δI (the bias current step) to calculate the voltage at the next point of the IV-characteristics. The final phase, voltage and magnetization components achieved at the previous point of the IV-characteristic are used as the initial conditions for the next current point. The voltage average V is given by $V = \frac{1}{T_f - T_i} \int V(t)dt$ where T_i and T_f determine the interval for the temporal averaging. The one-loop IV characteristic is obtained by sweeping the bias current from I= 0 to I= 3 and back down to I= 0. The initial condition for the magnetization components are $m_x = 0$, $m_y = 0.01$ and $m_z = \sqrt{(1 - m_x^2 - m_y^2)}$, while V_{in}=θ_{in}=0. The numerical parameter (if not mentioned) are $\alpha = 0.1$, $h_{ac} = 1$, $\phi_{sy} = \phi_{sz} = 4$ and $\Omega = \Omega_o = 0.5$.

3.1 Testing time discretization and numerical method stability

Before proceeding to investigate the dynamics for our system, it will be necessary to check the stability for numerical methods which we used. The system of equations which are mentioned in the last section have been solved using the 4^{th} order Rung-Kutta method. In this section numerical simulations are done with different time steps and average time domain for the integration. The following parameters are used: τ_j =1, $\Omega = \Omega_o = 0.5$, $h_{ac} = 1$, $\beta_c = 0.01$, $\alpha = 0.1$, $\phi_{sy} = \phi_{sz} = 4$ and step of current 0.005. The initial value for the magnetization components are $m_x = 0$, $m_y = 0.01$ and $m_z = \sqrt{1 - m_x^2 - m_y^2}$. We have two systems of equations one with $\epsilon_J = 0$ and a more complex one with $\epsilon_J \neq 0$. The scope of this part are limited to the time dependence for the total magnetization, one of the magnetization's component (e.g., m_x) and the voltage at different current value.

Figure.6 reveals the effect of changing the initial time on the magnetization and the voltage in case of ϵ_J =0. In this case, the solution of the LLG equation will be the same along the IV-curve. In Fig.6(a) The total magnetization is conserved over time such that $m = 1$ in dependent on T_i. However, the time dependence for the x-component of the magnetization and the voltage (as shown in Fig.6(b) and Fig.6(c) respectively), shows an instability for time less than 50. In Fig.6(b), the x-component of the magnetization for $T_i = 150$ (thick-black line) and $T_i = 200$ (dash dot- blue line) are coincides and out of phase with respect to the case of $T_i = 50$ (thin-red line). While the voltage at I=1.16 is changing in phase and amplitude according to T_i as shown in Fig.6(c).

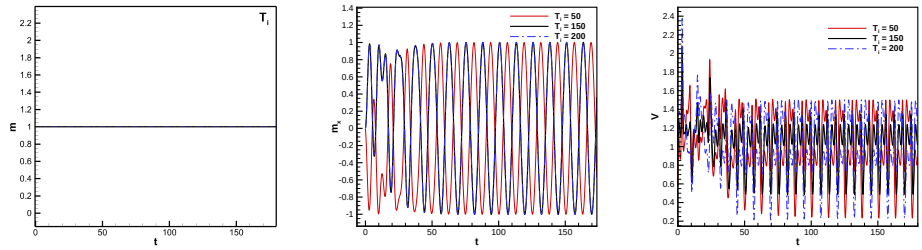

(a) (b) (c)

Figure 6: Time dependence of: (a) total magnetization, (b) x-component of magnetization and (c) voltage at ϵ_J=0, I=1.16 at three values of T_i = 50 (thin-red line), 150 (thick-black line) and 200(dash dot-blue line).

The next figure is devoted to the change of the discretization of time. Three values of T_P are taken (0.05,0.005,0.0005). Fig.7 shows the case with ϵ_J=0. It can be seen from Fig.7 (a) and Fig.7 (b) that the results are coincides for different step of time. In addition to this, the voltage time dependence at different current is shown in Fig.7 (c) where an instability occurs at t less than 50.

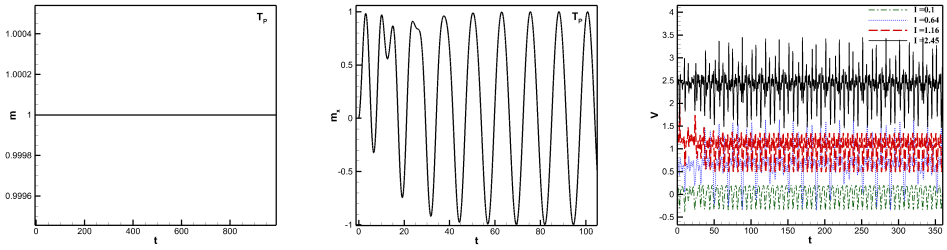

(a) (b) (c)

Figure 7: Time dependence of: (a) total magnetization, (b) x-component of magnetization and (c) voltage with ϵ_J=0, at three values of T_p = 0.05, 0.005 and 0.0005 (the results are coincides).

The case with $\epsilon_J \neq 0$ ($\epsilon_J = 2$) is shown in Fig.8. The results shown in the figure are all coincides for T_P equal to 0.05,0.005 and 0.0005. In addition to this, the behavior of the total, x-component of the magnetization and the voltage at different current, is shown in the figure. In Fig.8 (a) the total magnetization at I=0.1 (solid-blue line) and at I=0.64 (dotted-red line) equal to 1 along the whole time domain. However, changes in the 3^{rd} or 4^{th} digit after decimal point in m occur at I=1.16 (dashed-black line) and I=2.45 (dashed dot-green line) along the whole time domain of the calculations. Fig.8 (b) shows the x-component of the magnetization, for I=0.1 (solid-blue line) and I=0.64 (dotted-red line)

m_x=1 and -1 respectively. While at I=1.16 (dashed-black line) and I=2.45 (dashed dot-green line), m_x oscillates along the whole time domain. Fig.8 (c) shows the voltage time dependence, at I=0.1 (solid-blue line) and at I=0.64 (dotted-red line) the voltage average to zero. While at I=1.16 (dashed-black line) and I=2.45 (dashed dot-green line), the voltage averages to ≈ 1 and ≈ 2.5 respectively. An instability for t less than 200 occur for v at I=1.16.

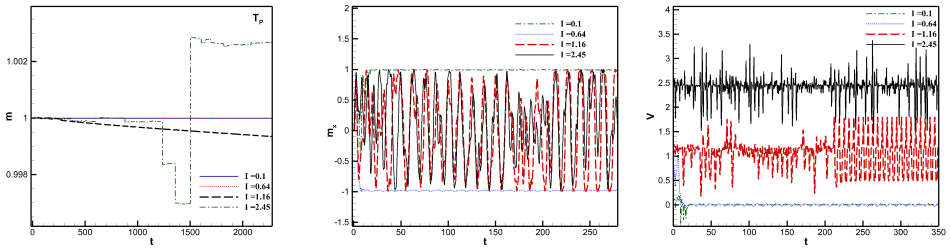

(a) (b) (c)

Figure 8: Time dependence of: (a) total magnetization, (b) x-component of magnetization and (c) voltage with ϵ_J=2, $T_p = 0.005$ and different values of I

Figure.9 demonstrates the effect of time step in case of external radiation with frequency $\omega = 0.5$ and amplitude $A = 0.3$ in case of ϵ_J=0. As shown in Fig.9(a), the total magnetization is conserved to 1. While for the x-component and voltage time dependence at I =1.16, oscillation occurs along the whole time domain of the calculations with instability for t less than 50. For both values of T_{P-rad} the oscillations are out of phase.

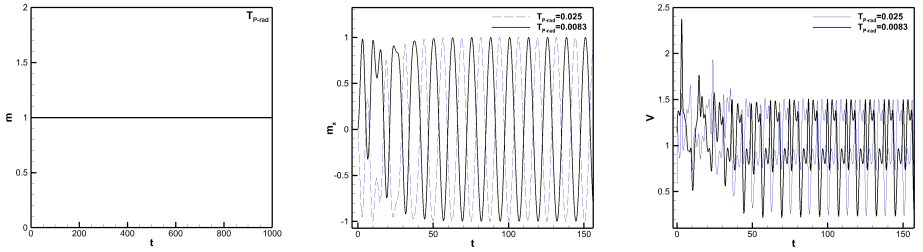

(a) (b) (c)

Figure 9: Time dependence of: (a) total magnetization, (b) x-component of magnetization and (c) voltage with ϵ_J=0, T_{p-rad} = 0.025 and 0.0083. The frequency of external radiation equal to 0.5 with amplitude 0.3

Other parameters e.g., average time for integration and step of current, do not bring changes in m, m_x and v.

3.2 Features of the IV-characteristic near and far from FMR

In this section, we are interested in investigating the effect of FMR on the IV-characteristic and magnetic moment components in the over-damped case $\beta_c = .01$. When $H_{eff} = H_o + H_{ac}$, the system of equations reduced to:

$$\begin{aligned}
\frac{dm_x}{d\tau} &= \frac{\Omega_o}{(1+\alpha^2)}\Big[\big(-m_y - \alpha m_x m_z\big) + \alpha h_{\rm ac}\cos(\Omega\,\tau)\big({m_y}^2 + {m_z}^2\big) \\
&+ h_{\rm ac}\sin(\Omega\,\tau)\big(-\alpha m_x m_y + m_z\big)\Big] \\
\frac{dm_y}{dt} &= \frac{\Omega_o}{(1+\alpha^2)}\Big[\big(m_x - \alpha m_y m_z\big) - h_{\rm ac}\cos(\Omega\,\tau)\big(\alpha m_x m_y + m_z\big) \\
&+ \alpha h_{\rm ac}\sin(\Omega\,\tau)\big({m_x}^2 + {m_z}^2\big)\Big] \\
\frac{dm_z}{dt} &= \frac{\Omega_o}{(1+\alpha^2)}\Big[\alpha\left({m_x}^2 + {m_y}^2\right) + h_{\rm ac}\cos(\Omega\,\tau)\big(m_y - \alpha m_x m_z\big) \\
&- h_{\rm ac}\sin(\Omega\,\tau)\big(m_x + \alpha m_y m_z\big)\Big]
\end{aligned} \tag{45}$$

which are solved with RSCJ equation. The following parameters are used: τ_j =1, Ω = 1, h_{ac} = 1, α = 0.1, $\phi_{sy} = \phi_{sz}$ = 4. The initial value for the magnetization components are m_x = 0, m_y = 0.01 and $m_z = \sqrt{(1 - m_x^2 - m_y^2)}$. Four different values for Ω_o are taken to be near and far from Ω = 1. Since the LLG equation in this case is not affected by the RCSJ equation, the magnetization components are the same along the IV-characteristic. Far from FMR e.g.,$\Omega_o = 0.1, 0.2$, the IV-characteristic has no significant differences from the usual case of RCSJ model in the over-damped case (see thick dashed-green line in Fig.10). While near and at FMR e.g.,Ω_o =0.7 and 1 respectively, voltage steps appear at 2*Ω and 4*Ω (thick dotted-black line and thick solid-blue line respectively). The width for these voltage steps in case of Ω_o = 0.7 is smaller than that in case of Ω_o = 1 (at FMR). The supper-current signals for different values of Ω_o show linear portions (increased when Ω_o close to Ω) at constant voltage steps (see thin- dashed, -dotted and -solid lines in Fig.10). Significant differences can be seen for magnetization component when resonance occur (see inset (I) and (II)). As shown in inset (I), the magnetization for m_x and m_y oscillates with small amplitude when Ω_o is far from Ω. While m_z decays and reach a value of $\approx$ 0.994. In inset (II) however, the magnetization of m_z reaches to a saturation value of zero. While the precession now lies in xy-plane. Another significant difference can be shown in insets (III) and (IV), where the

voltage time dependence is calculated for three different currents in the IV-characteristics. The voltage oscillation is not a sin wave when Ω_o is close to Ω but it is still periodic.

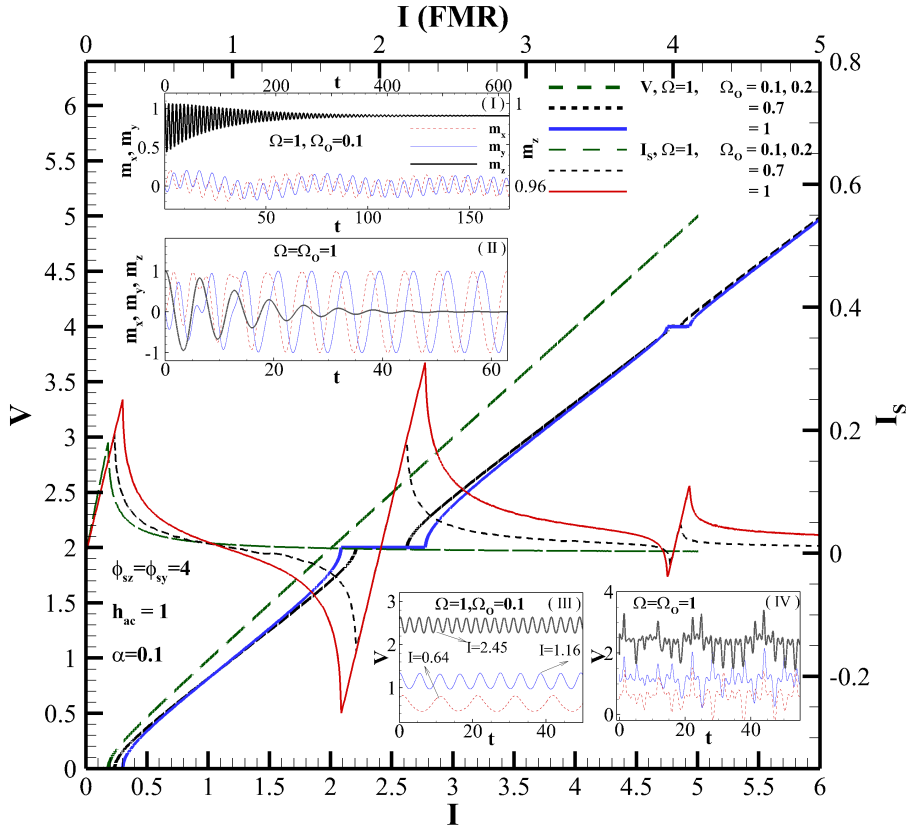

Figure 10: IV-characteristic for $\epsilon_J = 0$. For clarity, the x-axis at Ω_o =0.1,0.2 (far from FMR), represented by thick dashed-green line, is shifted with respect to Ω_o =0.7,1 (near and at FMR), which is represented by thick dotted-black line and thick solid-blue line respectively. The right y-axis is devoted to the supper-current signal corresponding to different values of Ω_o. Insets (I) and (II) indicate the time dependence of the magnetization component at Ω_o=0.1 and Ω_o=1 respectively. While insets (III) and (IV) represent the voltage time dependence at Ω_o=0.1 and Ω_o=1 respectively, for three-different current values at I=0.64 (dotted-red line), I=1.16 (thin solid-blue line) and I=2.45 (thick-black line) in the IV-characteristic.

The magnetization trajectory in 3D space is shown in Fig.11. As can be seen in inset (II) and (III), the magnetization follows paths in 3D till the magnetization in z-direction reach zero, then the trajectory path follows a constant circle in xy-plane of radius 1.

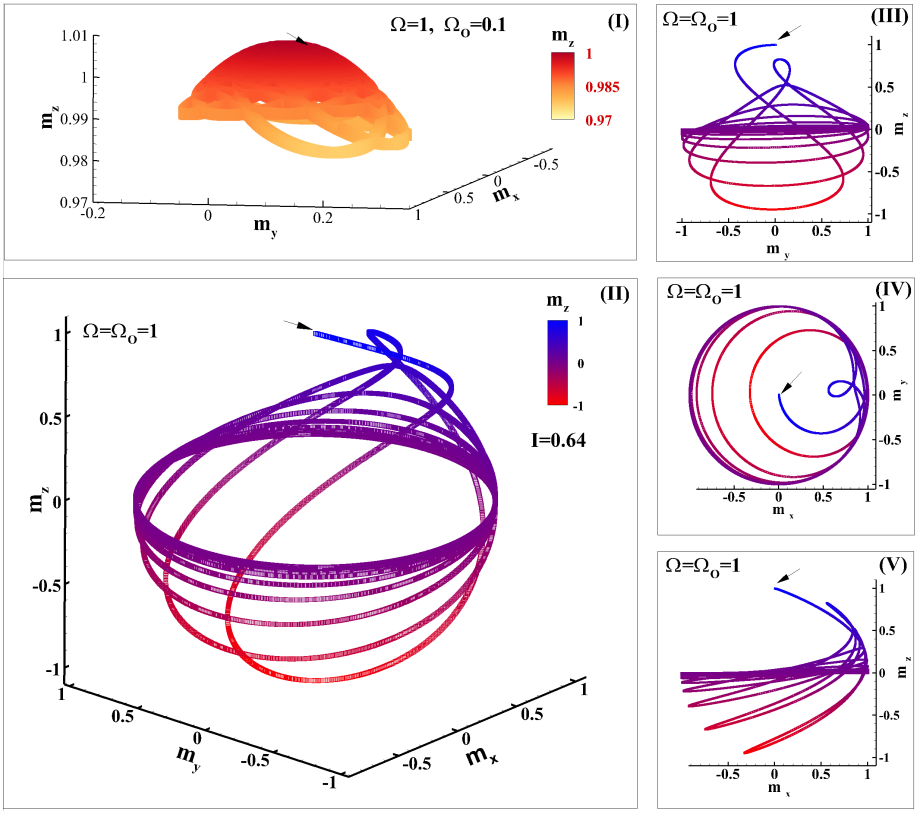

Figure 11: Magnetization trajectory at I= 0.64 and $\epsilon_J = 0$ in 3D space at $\Omega_o = 0.1$ (inset I) and $\Omega_o = 1$ (Inset II). Insets III, IV and V represent the 2D zy-, xy- and zx- plane respectively at $\Omega = \Omega_o = 1$. The arrows represent the starting point.

Now we switch to a more complicated case where $\epsilon_J \neq 0$. The dynamics of the system are determined by the system of equations.(**??**, **??**, **??**). Fig.12 represents the IV-characteristic and voltage time dependence in case of $\epsilon_J = 2$, $\alpha =_0 .16$ and $h_{ac} = 1.8$. Two cases are demonstrated in the figure. When $\Omega_o = 0.1, 0.2$ (Far from FMR), the IV-characteristic is similar to the usual over-damped case for Josephson junction (see thin dashed-green line). However, if $\Omega_o = 1$ (FMR), the IV-characteristic shows two voltage steps at 2*Ω and 4*Ω. In addition to this, several steps appear with different widths due the additional terms in LLG equation (ϵ_J terms). The supper-current signal reflects this. Linear portions in the supper-current signal corresponding to the constant voltage steps are seen in the figure (see thick-red line). The upward inset represents the voltage time dependence at different current values at $\Omega_o = 0.1$. When FMR occurs, these waves are changed dramatically as can be seen in the downward inset.

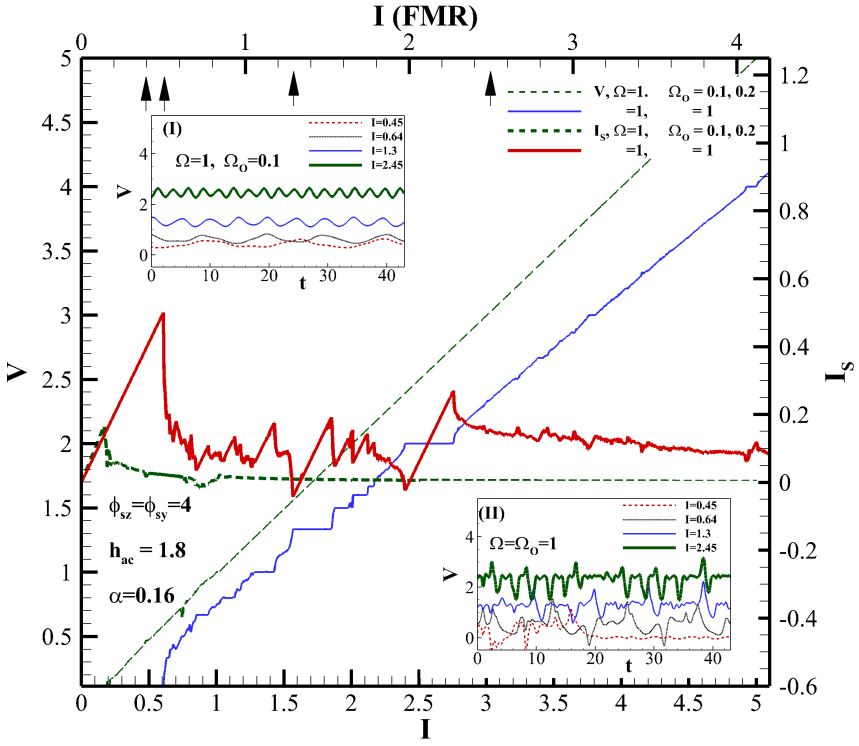

Figure 12: IV-characteristic for $\epsilon_J = 2$. For clarity, the x-axis at Ω_o =0.1,0.2 (far from FMR), represented by thin dashed-green line, is shifted with respect to Ω_o =1 (near and at FMR); which is represented by thin solid-blue line. The right y-axis is devoted to the supper-current signal corresponding to different values of Ω_o. Insets (I) and (II) indicate the voltage time dependence at Ω_o=0.1 and Ω_o=1 respectively, for four-different current values at I=0.45 (dashed-red line), I=0.64 (dotted-black line), I=1.3 (thin solid-blue line) and I=2.45 (thick-green line) in the IV-characteristic. The arrows represent the value of current in which the time dependence of the voltage and magnetization are determined.

Figure.13 demonstrates the time dependence of the magnetization at different current values (see arrows in Fig.12). The thick solid-green line represents the total magnetization to be sure than m=1 along the time domain of the calculations. In case of Ω_o far from FMR, no significant difference is observed for the magnetization components at different current values are seen in the upward insets. However, at FMR the magnetization components change dramatically and randomly. An interesting case occurs at I=0.45 and I=0.5, where we almost have a magnetization reversal in x-direction (see dotted-blue line in Fig.13 (a) and (b)).

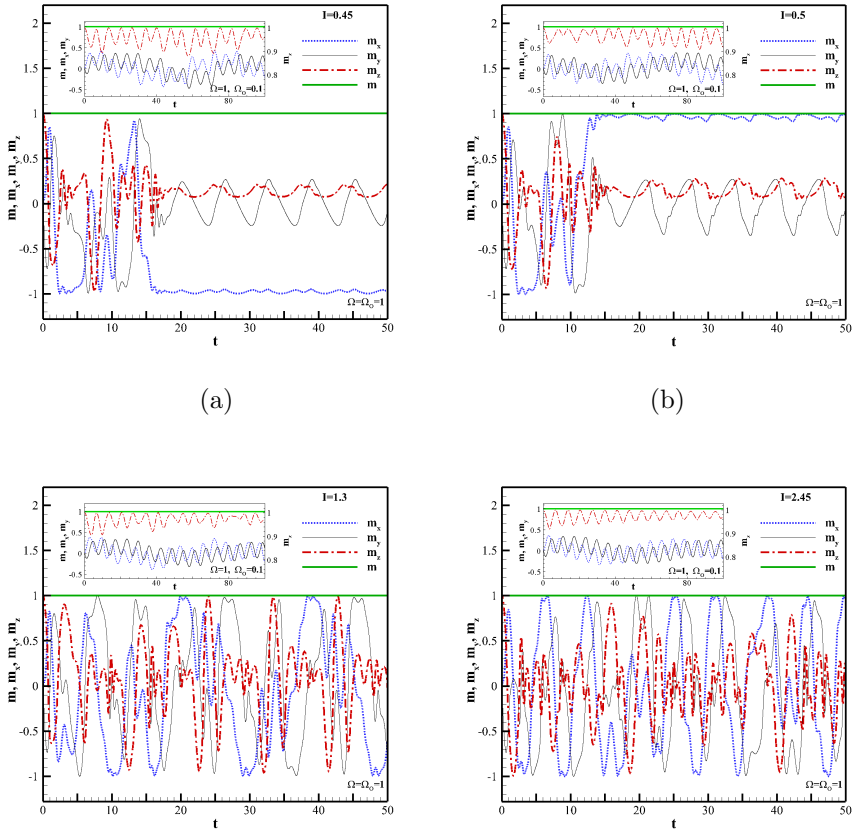

Figure 13: Magnetization time dependence when ϵ_J=2 at $\Omega_o = 0.1$ and $\Omega_o = 1$ for a) I=0.45, b) I=0.5, (c) I=1.3 and (d) I=2.45.

The total magnetization in the 3D space at different current values shows several trajectory paths. Figs (14,15,16,17,18,19) represent the trajectory of m at $\Omega_o = 0.1$ and $\Omega_o = 1$. At Ω_o=0.1 no significant change is occurred as can be seen in insets (I) in the figures. The total magnetization m lies on a sphere of radius 1. At I =0.64 (see Fig.16), the trajectory path draws almost a sphere of radius 1. While at I=2.45 (see Fig.19), not all the points of the sphere are covered; as can be seen in inset (IV) of the figure (i.e., points at the top and bottom of the sphere are not look like a preferred ones). At I=0.45 (Fig.14), I=0.5 (Fig.15), I=1.3 (Fig.17) and I=2.1 (Fig.18), it seems that the magnetization chooses a preferred paths.

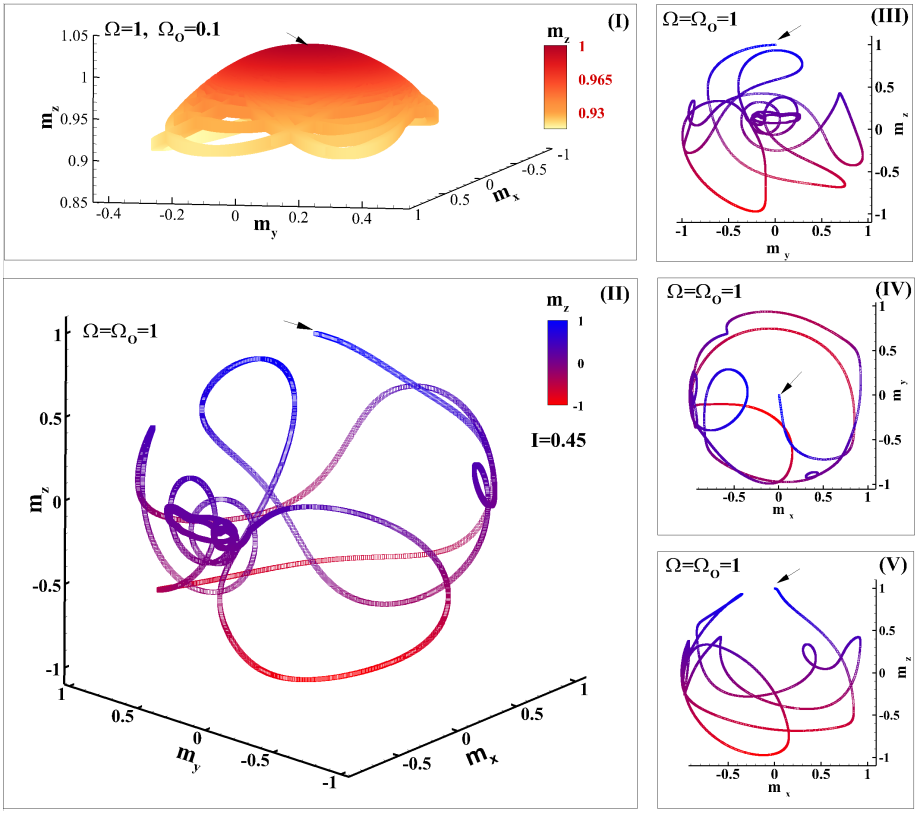

Figure 14: Magnetization trajectory at I= 0.45 and $\epsilon_J = 2$ in 3D space at $\Omega_o = 0.1$ (inset I) and $\Omega_o = 1$ (Inset II). Insets III, IV and V represent the 2D zy-, xy- and zx- planes respectively at $\Omega = \Omega_o = 1$. The arrows represent the starting point.

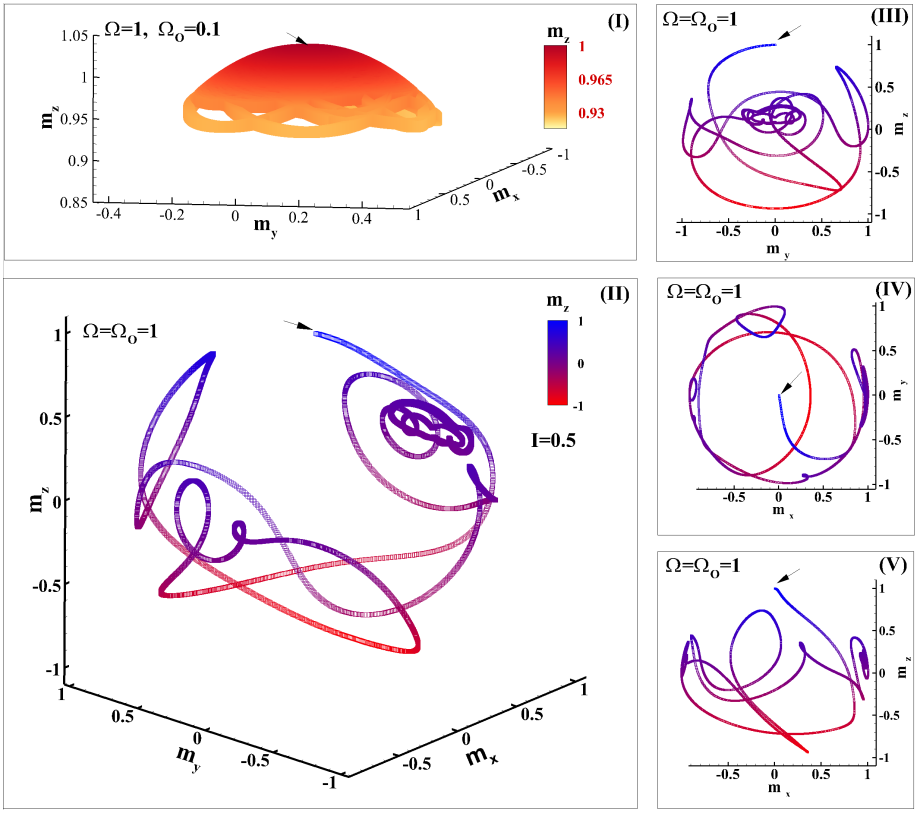

Figure 15: Magnetization trajectory at I= 0.5 and $\epsilon_J = 2$ in 3D space at $\Omega_o = 0.1$ (inset I) and $\Omega_o = 1$ (Inset II). Insets III, IV and V represent the 2D zy-, xy- and zx- planes respectively at $\Omega = \Omega_o = 1$. The arrows represent the starting point.

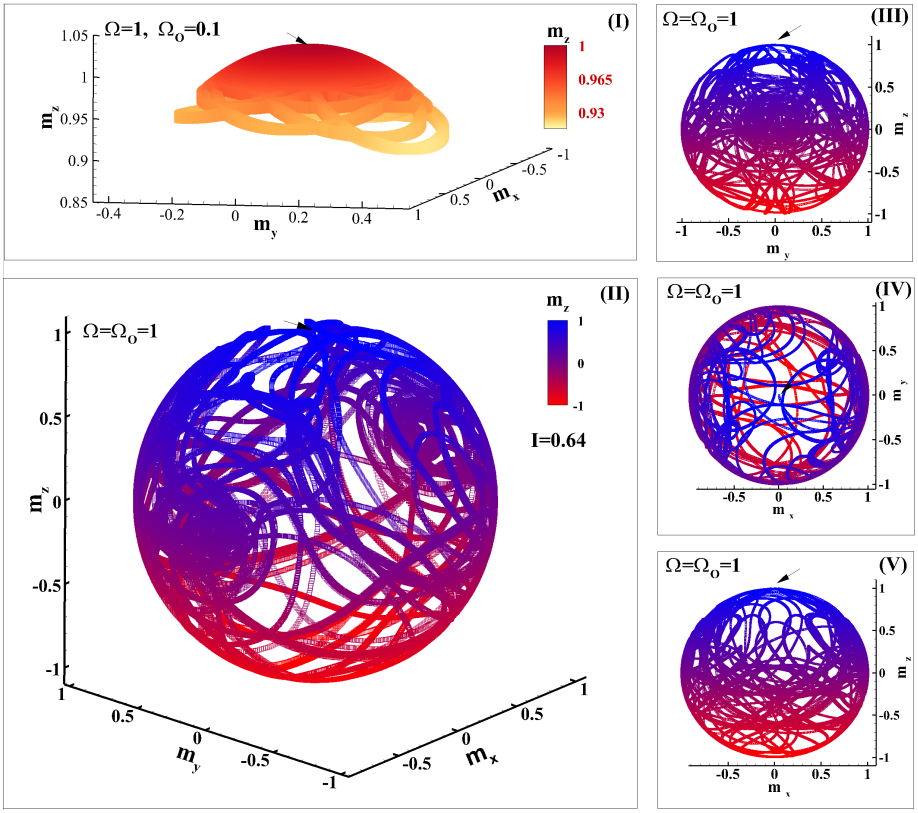

Figure 16: Magnetization trajectory at I= 0.64 and $\epsilon_J = 2$ in 3D space at $\Omega_o = 0.1$ (inset I) and $\Omega_o = 1$ (Inset II). Insets III, IV and V represent the 2D zy-, xy- and zx- planes respectively at $\Omega = \Omega_o = 1$. The arrows represent the starting point.

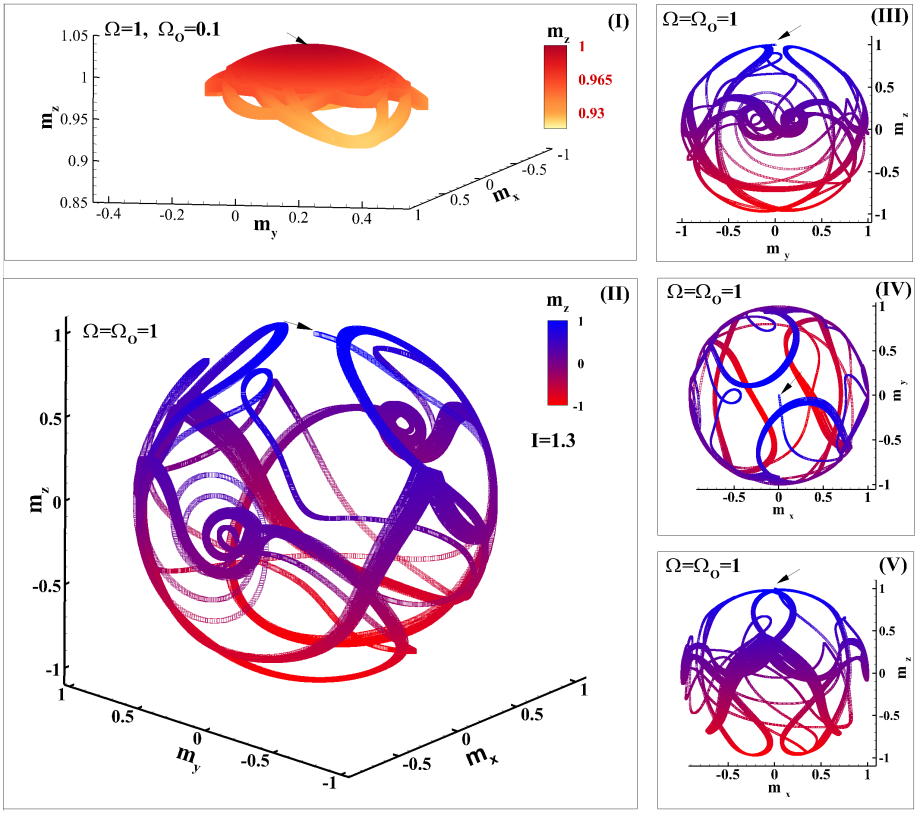

Figure 17: Magnetization trajectory at I= 1.3 and $\epsilon_J = 2$ in 3D space at $\Omega_o = 0.1$ (inset I) and $\Omega_o = 1$ (Inset II). Insets III, IV and V represent the 2D zy-, xy- and zx- planes respectively at $\Omega = \Omega_o = 1$. The arrows represent the starting point.

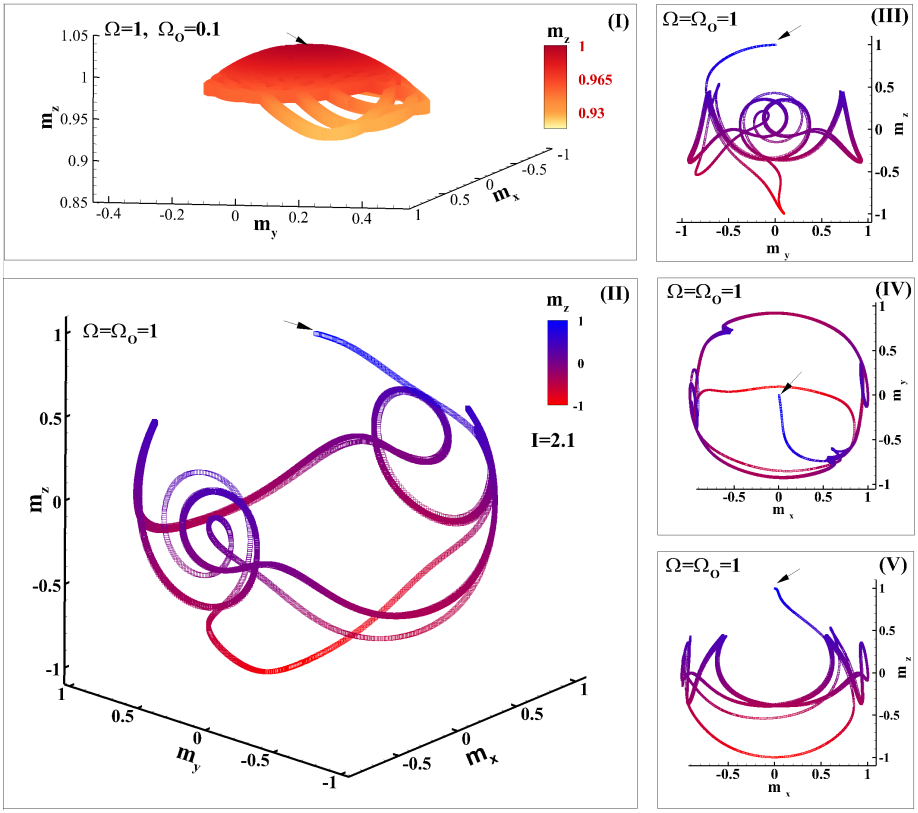

Figure 18: Magnetization trajectory at I= 2.1 and $\epsilon_J = 2$ in 3D space at $\Omega_o = 0.1$ (inset I) and $\Omega_o = 1$ (Inset II). Insets III, IV and V represent the 2D zy-, xy- and zx- planes respectively at $\Omega = \Omega_o = 1$. The arrows represent the starting point.

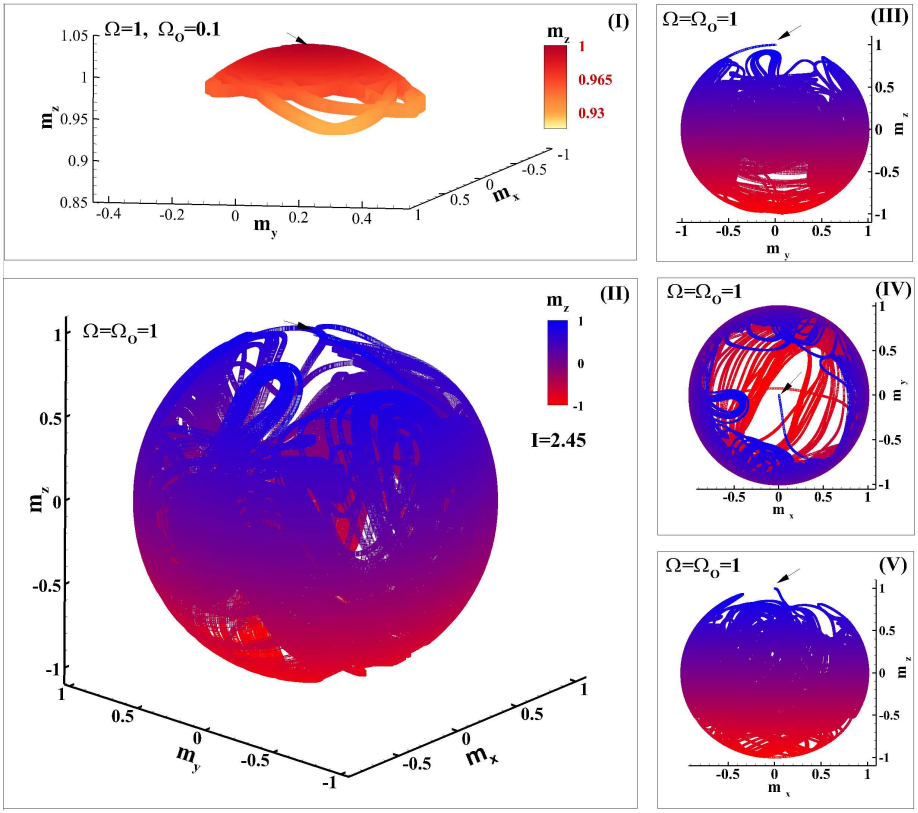

Figure 19: Magnetization trajectory at I= 2.45 and $\epsilon_J = 2$ in 3D space at $\Omega_o = 0.1$ (inset I) and $\Omega_o = 1$ (Inset II). Insets III, IV and V represent the 2D zy-, xy- and zx- planes respectively at $\Omega = \Omega_o = 1$. The arrows represent the starting point.

3.3 SFS Geometry

The effect of the SFS dimensions on the voltage steps due to FMR is demonstrated in [32] with $\beta_c = 0$. In Fig.20 we demonstrate the effect of ϕ_{sz} on the FMR steps. For the junction with $\phi_{sy} = \phi_{sz}$ we can see that the FMR steps have max width (see solid-blue line). By increasing the dimension of the junction in z-direction, the 2^{nd} FMR step is larger from the 1^{st} FMR step (see dotted-orange and dashed dotted-green lines). While for junctions with small dimension in z-direction, the 2^{nd} FMR width become very small of disappear (see dashed-black and solid-red lines). The critical current dependence on ϕ_{sz} is shown in Fig.21. In case of $\epsilon_J = 0$ and $= 0.2$, the critical current is look like Bessel functions. While at $\epsilon_J = 0.5$ a slight changes occur as can be seen by triangle-blue symbol in the figure.

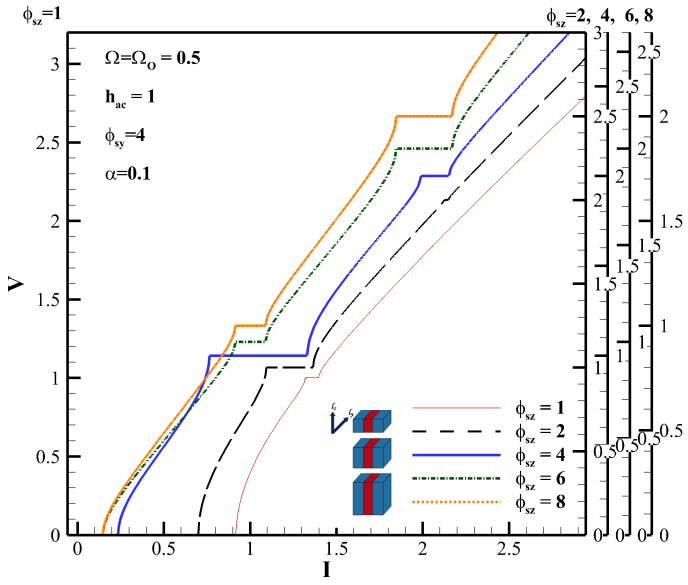

Figure 20: IV-characteristics for different values of ϕ_{sz} at FMR $\Omega = \Omega_o = 0.5$. For clarity the y-axises for different ϕ_{sz} are shifted with respect to each others.

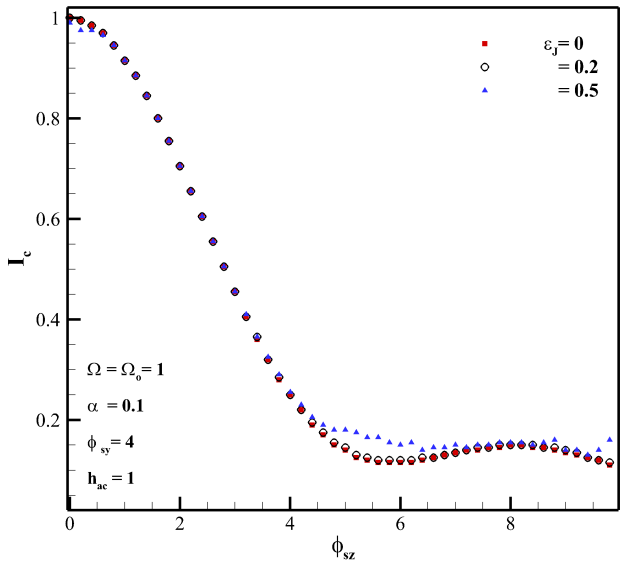

Figure 21: Critical current dependence on ϕ_{sz} at different values of ϵ_J.

Changing ϕ_{sy} at $\epsilon_J = 0$ does not bring significant change in the IV-characteristics.

At $\epsilon_J = 0.2$ the change in ϕ_{sy} and ϕ_{sz} brings significant changes in the IV-characteristic as can be seen in Fig.22. The voltage step widths and critical current are affected by ϕ_{sy} and ϕ_{sz} (see Fig.22.(a) and (b) respectively).

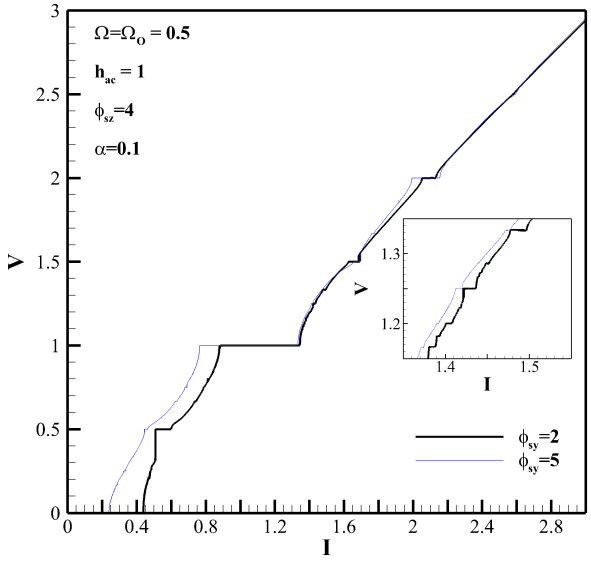

(a)

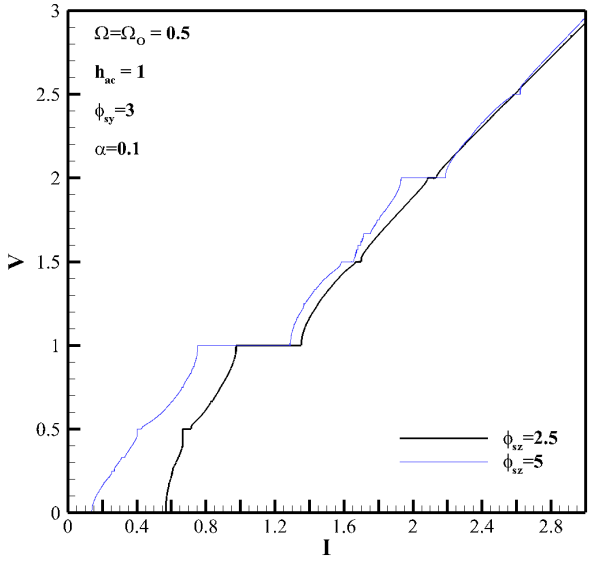

(b)

Figure 22: IV-characteristics at $\epsilon_J = 0.2$ with a) different ϕ_{sy} and b) ϕ_{sz}

3.4 External Radiation

In this section, the effect of external radiation with $\Omega = 0.5$ and A=0.4 is demonstrated in Fig.23. Four different cases are shown in the figure with y-axises shifted with respect to each other for clarity. The dotted-red line represents the case of no FMR with Ω, $\Omega_o = 3$ and $\epsilon_J = 0$. In this case, Shapiro steps appear at $V = 0.5, 1, 1.5$. The dashed-green line represents FMR case with $\Omega = \Omega_o = 0.5$ and $\epsilon_J = 0$. Here a significant change in the width of the steps occur. The width of the 2^{nd} step is larger than the 1^{st} step and additional steps appear at $V = 2, 2.5$. Same features is demonstrated in [32]. Now with $\epsilon_J = 0.25$ and $h_{ac} = 1$ (thin-blue line) we observe additional voltage steps with smaller widths. At $h_{ac} = 1.4$ (thick-black line) the width of these steps are increased.

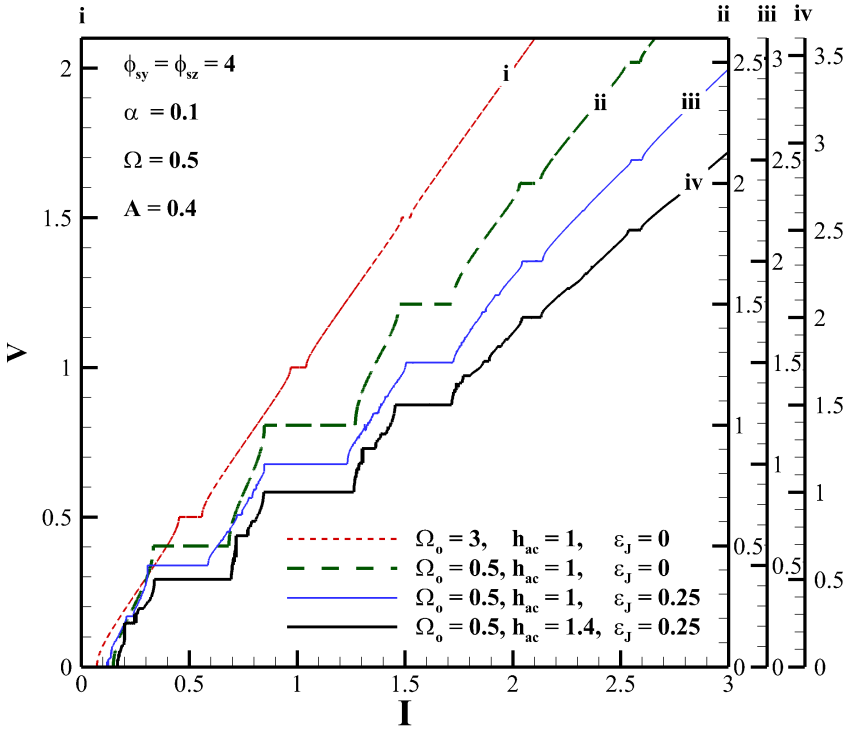

Figure 23: IV-characteristics with external radiation with $\Omega = 0.5$ and A=0.4. The y-axis for each case is shifted with respect to each other. The dotted-red line represents the case of no FMR with Ω, $\Omega_o = 3$ and $\epsilon_J = 0$. The dashed-green line represents FMR case with $\Omega = \Omega_o = 0.5$ and $\epsilon_J = 0$. The thin-blue line and thick-black line represent the case with $\epsilon_J = 0.25$ at $h_{ac} = 1$ and $h_{ac} = 1.4$ respectively.

The total magnetization trajectory in case of external radiation for the above four different cases at I=1.16 are shown in Fig.24. In Fig.(a) the total magnetization trajectory ends with a circle in xy-plane at $m_z \approx 0.8$. While at FMR, again the trajectory ends with a circle in xy-plane but now with $m_z \approx 0$ as

can be seen in Fig.(b). However, with $\epsilon_J = 0.25$ the circle is deformed slightly (quasi-2D). At $h_{ac} = 1.4$ slight changes occur for the trajectory, however it ends also with a deformed circle.

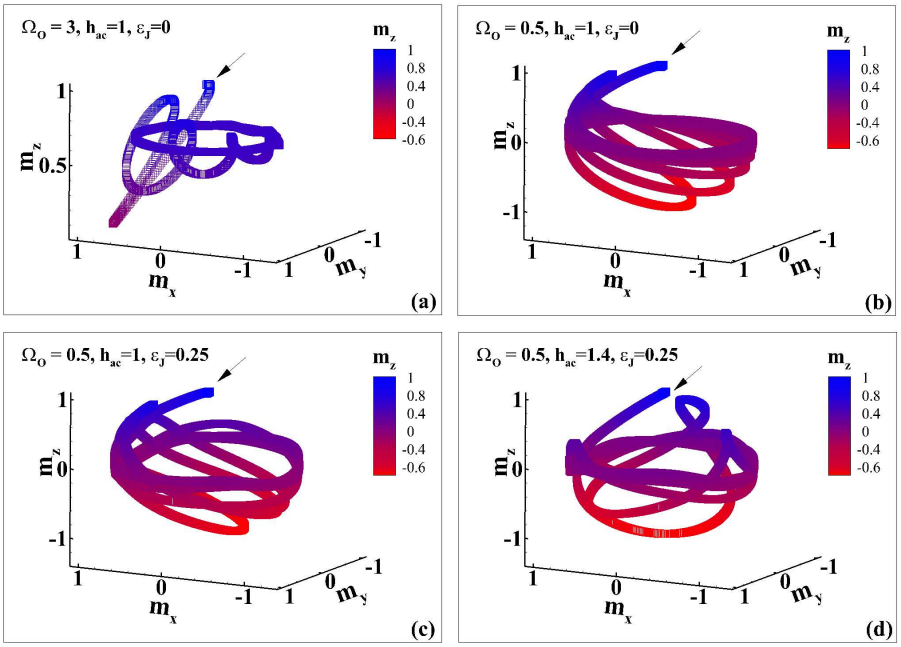

Figure 24: Total magnetization trajectory at different values of Ω_o, and ϵ_J.

The effect of the amplitude of the external radiation in the voltage steps at FMR is shown in Fig.25. The solid arrows represent the steps that coincides with FMR steps. While the hollow arrows represents the usual voltage steps. As shown in the figure the widths of these steps are changed dramatically with the amplitude of the external radiation. In [32] the dependence of the 1^{st} and 2^{nd} on the amplitude of the external radiation are studied in details.

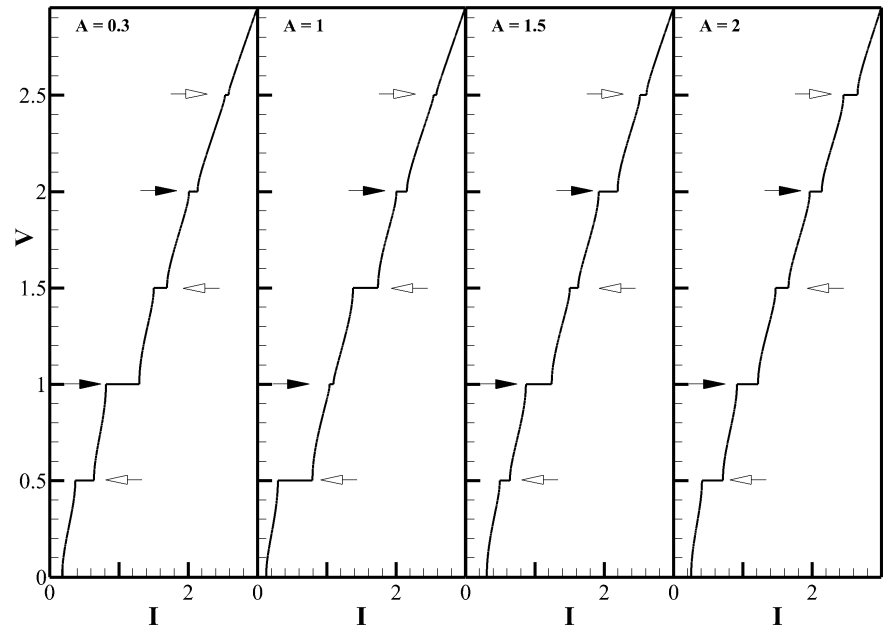

Figure 25: Voltage steps widths at different amplitude of the external radiation at $\epsilon_J = 0$.

4 Conclusions

To conclude, we develop model which describe spin wave coupling with Josephson phase in SFS junction based on RSCJ model. By solving nonlinear LLG equation with RSCJ together, we found new features related to coupling between Josephson phase and spin wave. We show that this coupling results in new interesting features of the I-V characteristics. Additional fractional voltage steps appears between FMR voltage steps which appear at $n\Omega$, n=2,4,6,...etc. The reason of the even number voltage steps is interpreted as follow: if the penetrating spin singlet Cooper pairs are scattered by the odd number of magnons, spin triplet state is formed, resulting in no Josephson current. While, if they scattered by even number of magnons spin singlet state is result, and the Josephson current flows. While the fractional voltage steps represent a series of fractional synchronization between the applied magnetic field frequency and the Josephson frequency. Josephson current manifests itself on the magnetization dynamics and induce large degree of nonlinearity to the magnetization trajectory. We demonstrate the effect of junction dimension on the voltage steps appears at FMR. Finally we show the effect of external radiation on the IV-characteristics when interaction between spin wave and Josephson phase is taken into account.

5 Acknowledgment

I would like to express my sincere gratitude to my advisor Prof. Yu. M. Shukrinov for the continuous support my research, for his patience, motivation, and immense knowledge. His guidance helped me in all the time of research and writing of this thesis. Besides my advisor, I would like to thank Dr. I. R. Rahmonov and Kirill Kulikov for their support.

My sincere thanks to Joint Institute for Nuclear Research (JINR) for giving me an opportunity to join this practice with a complete support, and gave me the access to the research facilities.

References

[1] Brian David Josephson. Possible new effects in superconductive tunnelling. *Physics letters*, 1(7):251–253, 1962.

[2] PW Anderson and JM Rowell. *Physical Review Letters*, 10(6):230–232, 1963.

[3] Hans Meissner. Superconductivity of contacts with interposed barriers. *Physical Review*, 117(3):672, 1960.

[4] VV Ryazanov, VA Oboznov, A Yu Rusanov, AV Veretennikov, Alexandre Avraamovitch Golubov, and J Aarts. Coupling of two superconductors through a ferromagnet: evidence for a π junction. *Physical review letters*, 86(11):2427, 2001.

[5] The current-phase relation in josephson junctions. *Reviews of modern physics*, 76(2):411, 2004.

[6] Jacob Linder and Jason WA Robinson. Superconducting spintronics. *arXiv preprint arXiv:1510.00713*, 2015.

[7] Igor Žutić, Jaroslav Fabian, and S Das Sarma. Spintronics: Fundamentals and applications. *Reviews of modern physics*, 76(2):323, 2004.

[8] Alexandre I Buzdin. Proximity effects in superconductor-ferromagnet heterostructures. *Reviews of modern physics*, 77(3):935, 2005.

[9] S Mai, E Kandelaki, AF Volkov, and KB Efetov. Interaction of josephson and magnetic oscillations in josephson tunnel junctions with a ferromagnetic layer. *Physical Review B*, 84(14):144519, 2011.

[10] Yu M Shukrinov, IR Rahmonov, K Sengupta, and A Buzdin. *arXiv preprint arXiv:1702.08394*, 2017.

[11] A Buzdin. *Physical review letters*, 101(10):107005, 2008.

[12] Liufei Cai and Eugene M Chudnovsky. *Physical Review B*, 82(10):104429, 2010.

[13] Liufei Cai, Dmitry A Garanin, and Eugene M Chudnovsky. *Physical Review B*, 87(2):024418, 2013.

[14] M Weides, M Kemmler, H Kohlstedt, R Waser, D Koelle, R Kleiner, and E Goldobin. 0- π josephson tunnel junctions with ferromagnetic barrier. *Physical review letters*, 97(24):247001, 2006.

[15] J Pfeiffer, M Kemmler, D Koelle, R Kleiner, E Goldobin, M Weides, AK Feofanov, J Lisenfeld, and AV Ustinov. Static and dynamic properties of 0, π, and 0- π ferromagnetic josephson tunnel junctions. *Physical Review B*, 77(21):214506, 2008.

[16] Shin-ichi Hikino, Michiyasu Mori, Saburo Takahashi, and Sadamichi Maekawa. Ferromagnetic resonance induced josephson current in a superconductor/ferromagnet/superconductor junction. *Journal of the Physical Society of Japan*, 77(5):053707–053707, 2008.

[17] AF Volkov and KB Efetov. Hybridization of spin and plasma waves in josephson tunnel junctions containing a ferromagnetic layer. *Physical review letters*, 103(3):037003, 2009.

[18] Konstantin Konstantinovich Likharev. *Dynamics of Josephson junctions and circuits*. Gordon and Breach science publishers, 1986.

[19] Antonio Barone and Gianfranco Paterno. *Physics and applications of the Josephson effect*, volume 1. Wiley Online Library, 1982.

[20] Lev Davidovich Landau and EM Lifshitz. *Course of Theoretical Physics. Vol. 8: Electrodynamics of Continuous Media*. Oxford, 1960.

[21] Robert L. Stamps Robert E. Camley, Zbigniew Celinski. *Handbook of Surface Science,Magnetism of Surfaces, Interfaces, and Nanoscale Materials, Volume 5*. Elsevier Press, 2015.

[22] Yu M Shukrinov, S Yu Medvedeva, AE Botha, MR Kolahchi, and A Irie. Devil's staircases and continued fractions in josephson junctions. *Physical Review B*, 88(21):214515, 2013.

[23] BD Josephson. *Superconductivity*, 1:423–447, 1969.

[24] John R Waldram. *Superconductivity of metals and cuprates*. CRC Press, 1996.

[25] WC Stewart. *Applied Physics Letters*, 12(8):277–280, 1968.

[26] DE McCumber. *Journal of Applied Physics*, 39(7):3113–3118, 1968.

[27] Israel D Vagner, Boris I Lembrikov, and Peter Rudolf Wyder. *Electrodynamics of magnetoactive media*, volume 135. Springer Science & Business Media, 2004.

[28] Franz Schwabl. *Statistical mechanics*. Springer Science & Business Media, 2010.

[29] Bernard Dieny, Ronald B Goldfarb, and Kyung-Jin Lee. *Introduction to magnetic random-access memory*. John Wiley & Sons, 2016.

[30] TL Gilbert. A lagrangian formulation of the gyromagnetic equation of the magnetization field. *Phys. Rev.*, 100:1243, 1955.

[31] K Ounadjela and B Hillebrands. Spin dynamics in confined magnetic structures ii, 2003.

[32] S Hikino, M Mori, S Takahashi, and S Maekawa. *Superconductor Science and Technology*, 24(2):024008, 2011.

[33] Alexander G Gurevich and Gennadii A Melkov. *Magnetization oscillations and waves*. CRC press, 1996.